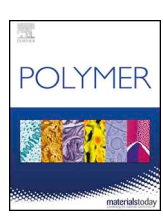


#### Contents lists available at ScienceDirect

### Polymer

journal homepage: www.elsevier.com/locate/polymer



## Reinforcement of polychloroprene by grafted silica nanoparticles



Zaid M. Abbas<sup>a,b</sup>, Massimo Tawfilas<sup>c</sup>, Mohammed M. Khani<sup>a</sup>, Karl Golian<sup>a</sup>, Zachary M. Marsh<sup>a</sup>, Mayank Jhalaria<sup>d</sup>, Roberto Simonutti<sup>c</sup>, Morgan Stefik<sup>a</sup>, Sanat K. Kumar<sup>d</sup>, Brian C. Benicewicz<sup>a,\*</sup>

- <sup>a</sup> Department of Chemistry and Biochemistry, University of South Carolina. Columbia, South Carolina, 29208, United States
- <sup>b</sup> Department of Chemistry, Wasit University, Hay Al-Rabea, Kut, Wasit, 52001, Iraq
- <sup>c</sup> Department of Materials Science, University of Milano-Bicocca, Via R. Cozzi 55, 20125, Milano, Italy
- d Department of Chemical Engineering, Columbia University, New York, NY, 10027, United States

#### HIGHLIGHTS

- Polychloroprene grafted nanoparticles were prepared with precise control of graft density, molar mass and dispersity.
- Correlations were made between dispersion state in an industrial rubber andmechanical properties.
- High molar mass grafts and low chain density provided the best dispersion and largest improvements in mechanical properties.

#### ARTICLE INFO

# Keywords: Polychloroprene RAFT polymerization Nanocomposites Surface modification

#### ABSTRACT

Reversible addition-fragmentation chain transfer polymerization of chloroprene on the surface of silica nanoparticles was performed to obtain polychloroprene-grafted-silica nanoparticles (PCP-g-SiO<sub>2</sub> NPs). These particles were dispersed in a commercial polychloroprene matrix to obtain PCP nanocomposites with different silica core loadings (1, 5, 10, and 25 wt%). Two different chain graft densities were studied ("low," 0.022 ch/nm² and "high," 0.21 ch/nm²) as a function of the grafted polymer molecular mass. The cured samples showed significant improvement in the mechanical properties of the PCP rubber nanocomposites as compared to the unfilled PCP as measured by standard tensile and dynamic mechanical analysis even with low silica content. The mechanical properties of the nanocomposites were notably enhanced when the graft density was low and grafted molecular masses were high. Transmission electron microscopy (TEM) and Small-Angle X-ray Scattering (SAXS) were used to analyze the dispersion states of the grafted nanoparticles which confirmed the correlation between high grafted chain lengths and improved dispersion states and mechanical properties.

#### 1. Introduction

Mechanical reinforcement of rubber materials by inorganic fillers has been practiced for many years [1–5]. Carbon black and metal oxides are the most popular types of fillers that have been used in rubber nanocomposites [6–10]. The interactions between the inorganic fillers and polymeric matrix exert a strong influence on the properties of the final composite [11,12]. The reinforcement materials and procedures used in the preparation of nanocomposites are very important factors to the understanding of their structure–property relationships, especially the method of attaching the polymer brushes to the surface of inorganic nanomaterials [13–15]. One of the main research areas in using inorganic fillers in rubbery matrices has been to lower the phase separation of the inorganic particles [16]. Many early attempts used

modified fillers containing some organic functional groups that were miscible or could react with the matrix to minimize the agglomeration of the fillers. More recent efforts have carefully examined many molecular variables such as graft chain density, particle loading and ligand choice which can influence the composite properties [17–19]. The reinforcements of the rubber materials have been focused on the improvement of stiffness, modulus, rupture energy, tear strength, tensile strength, cracking resistance, fatigue resistance, and abrasion resistance [20].

A critical aspect of the presence of a filler is the strength of interaction between a chemically grafted filler particle and the matrix [21]. The major factors that control the reinforcing mechanism of inorganic fillers in rubber matrices are the dispersion into the matrix and the interaction between rubber and fillers [22]. Various functional groups

E-mail address: Benice@sc.edu (B.C. Benicewicz).

<sup>\*</sup> Corresponding author.

have been used to passivate the surface of the inorganic fillers including silanes, phosphonates, amines, hydroxides, and alkyl groups. However, many of the previous studies still resulted in agglomeration and aggregation of the fillers due to particle-matrix incompatibility [23,24].

Polychloroprene (PCP) was discovered by Dupont (1931) and has been widely used in the rubber industry [25]. It can be vulcanized with sulfur, organic peroxides and metal oxides to produce sheets and films with good elasticity, perspiration, resistance to oil and various solvents, excellent weatherability, and excellent thermal and thermoxidative stability [26]. It is particularly noted for its durability when exposed to multiple degradation modes.

In this work, silica nanoparticles with grafted PCP chains were used as hybrid fillers in PCP matrices to improve the composite properties. Strong rubber-filler interactions lead to increased strength in rubber composites. A bound rubber model was suggested in several reports where tightly and loosely bound rubber, surrounding the filler particles, had been shown to act as an additional crosslink mechanism in the rubber matrix [23,27]. Bound rubber represents the bonds of rubber chains to the inorganic particles being strong enough to persist in the final composite [7,28]. However, most studies focus on the use of small surface functional groups to enhance the interactions [29,30]. Our previous work has shown that the molecular weight and graft density of grafted chains can also be used to control the dispersion of nanoparticles in polymer matrices, as well as the strength of interactions [31-33]. To expand on this concept in the current study, we explored two different polymer graft densities, four silica loading levels (1, 5, 10, 25 wt%) and a broad range of grafted molecular weights (34.8-161 kDa). The use of these grafted nanoparticles in cured composites showed improvements for filled samples even at low silica loadings (1 wt%). Furthermore, the high grafted molecular weights (161 kDa and 134 kDa) enhanced the final composite properties more than low grafted molecular weights (38 kDa and 34.8 kDa), and the low graft densities (0.022 ch/nm<sup>2</sup>) were better than the high graft densities  $(0.21 \text{ ch/nm}^2).$ 

#### 2. Experimental

#### 2.1. Materials

Chloroprene monomer was prepared through dehydrochlorination of 3,4-dichloro-1-butene purchased from TCI America [20,34]. The RAFT agent 2-methyl-2-(dodecylsulfanylthiocarbonyl)sulfanyl] propanoic acid (MDSS) (97%) was purchased from Strem Chemicals and used as received. Spherical silica nanoparticles ( $SiO_2$ ) with a diameter of 14  $\pm$  4 nm were purchased from Nissan Chemical Co. Tetrahydrofuran (THF) (HPLC grade, Fisher), aminopropyldimethylethoxysilane (APS), octyldimethylethoxysilane (ODMES) and octadecyldimethylethoxysilane (C18) were purchased from Gelest (95%) and used as received. Tetrabutylammonium bromide (PTC, 99%) was purchased from Oakwood Chemicals and used as received. 2.2'-Azobisisobutyronitrile (AIBN) was purified by recrystallization from methanol and dissolved in THF to make a 10 mM solution. PCP 150K was purchased from Sp2 polymers. All other reagents were used as received.

#### 2.2. Synthesis of alkyl silane-grafted-SiO<sub>2</sub> (C18 NPs)

A solution (10 mL) of colloidal silica particles (30 wt % in methyl isobutyl ketone) was added to a 250 mL round bottom (r.b.) flask equipped with a condenser and diluted with 30 mL of THF. Octadecyldimethylethoxysilane (C18) (1 g,  $2.92 \, \mathrm{mmol}$ ) was added to the mixture and refluxed in a 75 °C oil bath for  $12 \, \mathrm{h}$  under flowing nitrogen. The reaction was then cooled to room temperature (r.t.) and precipitated in methanol ( $120 \, \mathrm{mL}$ ). The particles were recollected by centrifugation ( $5000 \, \mathrm{rpm}$ ) and dispersed in THF using sonication ( $5 \, \mathrm{min}$ ) and precipitated in methanol again. The C18-functionalized particles were then dispersed in  $40 \, \mathrm{mL}$  of THF.

#### 2.3. Synthesis of chloroprene monomer (Scheme S1)

Chloroprene monomer was prepared by placing NaOH (16 g, 0.404 mol), PTC (4.35 g, 0.0134 mol) and 65 mL of water into a 250 mL three-necked r.b. flask. A condenser was fitted, and the mixture was stirred and heated. At 55 °C, 3,4-dichloro-1-butene (25 g, 0.2 mol) was added dropwise over 5 min. Heating was continued and the product was distilled as a hazy liquid; 60–75 °C for 2 h. Drying over MgSO<sub>4</sub> yielded a clear, colorless liquid. Chloroprene monomer is self-polymerizing under ambient conditions and was stabilized by adding 0.1% (w/w) phenothiazine stabilizer to the dried product and the solution purged with nitrogen. Yields 74%.  $^1\mathrm{H}$  NMR (400 MHz, CDCl<sub>3</sub>)  $\delta$  5.22–5.25 (2H, d, CH<sub>2</sub>=CH), 5.31–5.34 (2H, d, CH<sub>2</sub>=CCl), 6.31–6.40 (1H, q, CCl–CH) (Fig. S1). HRMS (EI) (m/z) calcd for C<sub>4</sub>H<sub>5</sub>Cl: 88.0080; found: 88.0110 [34].

# 2.4. Synthesis of dodecyl (2-methyl-1-oxo-1-(2-thioxothiazolidin-3-yl) propan-2-yl) carbonotrithioate (activated-MDSS) (Scheme S2)

The procedure for the activation of MDSS is given below, similar to that previously reported [3]. MDSS (2 g, 5.49 mmol), N,N'-dicyclohexylcarbodiimide (1.24 g, 6.03 mmol) and 2-mercaptothiazoline (0.718 g, 6.03 mmol) were dissolved in dichloromethane (40 mL) in a 100 mL r.b. flask under a nitrogen stream. After 10 min at r.t., a solution of 4-dimethylaminopyridine (0.067 g, 0.549 mmol) dissolved in dichloromethane (2 mL) was added to the mixture and the nitrogen flow was removed. After 5 h at r.t., the mixture was filtered, and the solvent evaporated using a rotary evaporator. The product was purified by column purification using a silica column with 5:4 ethyl acetate:hexane. Yields were usually greater than 80%, m.p. 98.1 °C (Fig. S2), <sup>1</sup>H NMR (400 MHz, CDCl<sub>3</sub>) δ 3.21 (2H, t, S-CH<sub>2</sub>-(CH2)<sub>10</sub>-CH<sub>3</sub>), 1.6 (6H, s, C-(CH<sub>3</sub>)<sub>2</sub>), 1.19-1.31 (16H, t, -(CH<sub>2</sub>)<sub>8</sub>-CH<sub>3</sub>), 1.58 (2H, m, CH<sub>2</sub>-(CH<sub>2</sub>)<sub>8</sub>-CH<sub>3</sub>), 2.06 (2H, m, -CH<sub>2</sub>-CH<sub>2</sub>-(CH<sub>2</sub>)<sub>8</sub>-CH<sub>3</sub>) 0.81 (3H, t, SCH<sub>2</sub>- $(CH2)_{10}-CH_3)$ , 3.51 (2H, t, N-CH<sub>2</sub>-CH<sub>2</sub>-S), 3.91 (2H, t, S- $\oplus$  $CH_2-CH_2-N$ ) (Fig. S3).

#### 2.5. Synthesis of MDSS-g-SiO<sub>2</sub>

A solution (10 mL) of silica nanoparticles (30 wt % in methyl isobutyl ketone) was added to a 100 mL r.b. flask and diluted with 15 mL of THF. Octyldimethylethoxysilane (ODMES) (0.3 mL, 1.21 mmol) was added to the mixture and refluxed in a 75 °C oil bath for 12 h under flowing nitrogen. The reaction was cooled to r.t. and precipitated in hexanes (120 mL). The particles were collected by centrifugation and dispersed in THF (20 mL) using sonication and precipitated in hexanes again. The ODMES-functionalized particles were dissolved in THF (20 mL), combined with 3-aminopropyldimethylethoxysilane (APS) and the mixture was refluxed in a 75 °C oil bath for 3 h under flowing nitrogen. The reaction was then cooled to r.t. and precipitated in hexanes (120 mL). The particles were recollected by centrifugation and dispersed in THF using sonication and precipitated in hexanes again. The amine-functionalized particles were dispersed in 40 mL of THF for further reaction. Then predetermined weight of activated MDSS was added dropwise at r.t. to a THF solution of the amine functionalized silica nanoparticles (Table S1). After complete addition, the solution was stirred overnight. The reaction mixture was then precipitated into 400 mL of hexanes. The particles were recollected by centrifugation at 3000 rpm for 8 min. The particles were redispersed in 30 mL THF and precipitated in hexanes. This dissolution-precipitation procedure was repeated 2 more times until the supernatant layer after centrifugation was colorless. The yellow MDSS-anchored silica nanoparticles were dried under vacuum at r.t. and analyzed using UV analysis to determine the chain density using a calibration curve constructed from standard solutions of free MDSS (see SI, Table S2, Fig. S4) [35-37].

 Table 1

 Sample details and properties of cured PCP nanocomposites.

Sample name	Mn (kDa) <sup>a</sup>	Graft density (ch/nm²)	Silica <sup>b</sup> loading(wt %)	Tensile strength (MPa)	Elongation at Break (%)	Degree of Swelling(%)	Crosslink Densit (v*10 <sup>4</sup> mol/cc)
PCP Unfilled	150	-	0	2.2 ± 1.1	5.3 ± 1.1	491 ± 5	0.52 ± 0.01
C18-1%	0	-	1	$2.6 \pm 0.7$	$4.9 \pm 1.0$	$486 \pm 9$	$0.58 \pm 0.02$
38k-1%	38	0.21	1	$2.6 \pm 0.1$	$5.8 \pm 1.1$	481 ± 11	$0.59 \pm 0.02$
73k-1%	73	0.21	1	$3.4 \pm 1.0$	$6.3 \pm 0.5$	$461 \pm 7$	$0.63 \pm 0.02$
161k-1%	161	0.21	1	$4.7 \pm 0.7$	$8.8 \pm 0.8$	$442 \pm 12$	$0.68 \pm 0.03$
C18-5%	0	-	5	$3.2 \pm 0.8$	$6.3 \pm 0.3$	$462 \pm 3$	$0.58 \pm 0.01$
38k-5%	38	0.21	5	$4.6 \pm 0.8$	$7.5 \pm 1.2$	$445 \pm 4$	$0.63 \pm 0.01$
73k-5%	73	0.21	5	$4.3 \pm 1.7$	$7.5 \pm 1.9$	429 ± 15	$0.69 \pm 0.03$
161k-5%	161	0.21	5	$6.0 \pm 0.5$	$10.8 \pm 0.3$	$411 \pm 2$	$0.72 \pm 0.01$
34.8k-5%	34.8	0.022	5	$7.4 \pm 1.5$	$7.2 \pm 0.6$	$438 \pm 15$	$0.64 \pm 0.04$
134k-5%	134	0.022	5	$7.4 \pm 2.8$	$7.4 \pm 2.0$	$407 \pm 5$	$0.74 \pm 0.01$
C18-10%	0	_	10	$4.4 \pm 1.0$	$6.9 \pm 1.0$	$429 \pm 12$	$0.61 \pm 0.05$
38k-10%	38	0.21	10	$4.7 \pm 0.4$	$8.3 \pm 0.4$	$400 \pm 3$	$0.68 \pm 0.01$
73k-10%	73	0.21	10	$5.6 \pm 1.0$	$10.3 \pm 1.0$	$389 \pm 11$	$0.72 \pm 0.05$
161k-10%	161	0.21	10	$6.9 \pm 1.0$	$12.9 \pm 1.3$	$341 \pm 6$	$0.91 \pm 0.02$
34.8k-10%	34.8	0.022	10	$6.7 \pm 1.0$	$6.8 \pm 1.0$	$381 \pm 4$	$0.74 \pm 0.01$
134k-10%	134	0.022	10	$7.8 \pm 1.1$	$8.8 \pm 0.8$	$361 \pm 11$	$0.81 \pm 0.04$
C18-25%	0	-	25	$5.0 \pm 2.0$	$9.2 \pm 0.4$	$311 \pm 6$	$0.67 \pm 0.02$
34.8k-25%	34.8	0.022	25	$7.9 \pm 1.4$	$9.4 \pm 0.6$	$225 \pm 7$	$1.15 \pm 0.06$
134k-25%	134	0.022	25	$8.9 \pm 1.2$	$9.5 \pm 0.4$	166 ± 10	$1.91 \pm 0.19$

All composites dispersed in 150 kDa PCP.

<sup>&</sup>lt;sup>b</sup> Silica loading calculated to total polymer plus silica.

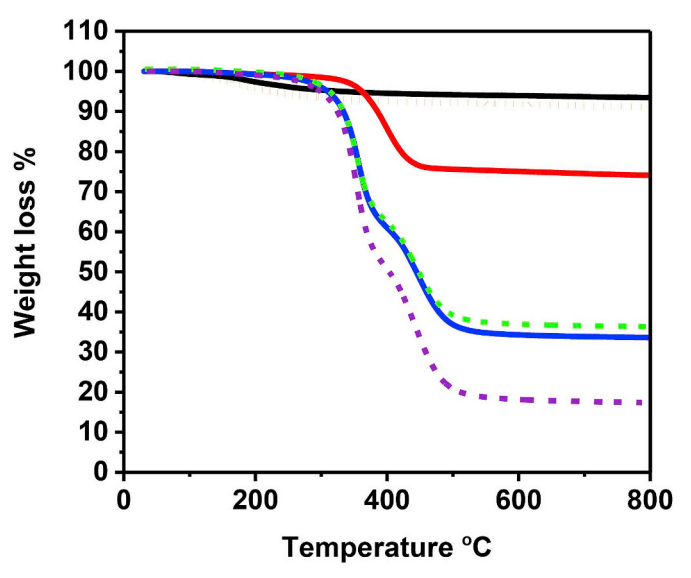


**Fig. 1.** TGA results for low density RAFT agent attached NPs  $0.022 \, \text{ch/nm}^2$  (black line), 34.8k graft on  $0.022 \, \text{ch/nm}^2$  (red line), 34.8k-25% cured composites (blue line), high density RAFT agent attached NPs  $0.21 \, \text{ch/nm}^2$  (orange dash line), 38k graft on  $0.21 \, \text{ch/nm}^2$  (green dash line) and 38k-10% cured composites (purple dash line). (For interpretation of the references to color in this figure legend, the reader is referred to the Web version of this article.)

#### 2.6. Procedures for surface-initiated RAFT polymerization of chloroprene

Chloroprene (1 g) with MDSS-g-SiO<sub>2</sub> as the RAFT agent (0.22 g 0.21 ch/nm²), AIBN (114  $\mu$ l from 10 mM stock solution) with reaction ratio [1000:1:0.1, (monomer: CTA: initiator)] and THF (3 ml) were added and mixed well in a Schlenk tube. The mixture was degassed by three freeze-pump-thaw cycles, filled with nitrogen, and the Schlenk flask was placed in an oil bath at 60 °C for 48 h. The resulting PCP grafted particles were precipitated into a large amount of methanol and centrifuged at 8,000 rpm for 10 min and redispersed in THF. After cleaving the chains from the silica NPs, the molecular weight of the grafted chains was 38 kDa. Different molecular weights were synthesized by varying the [monomer: CTA: initiator] ratio and time (Table S3) [38]. After polymerization the RAFT agent attached to the chain

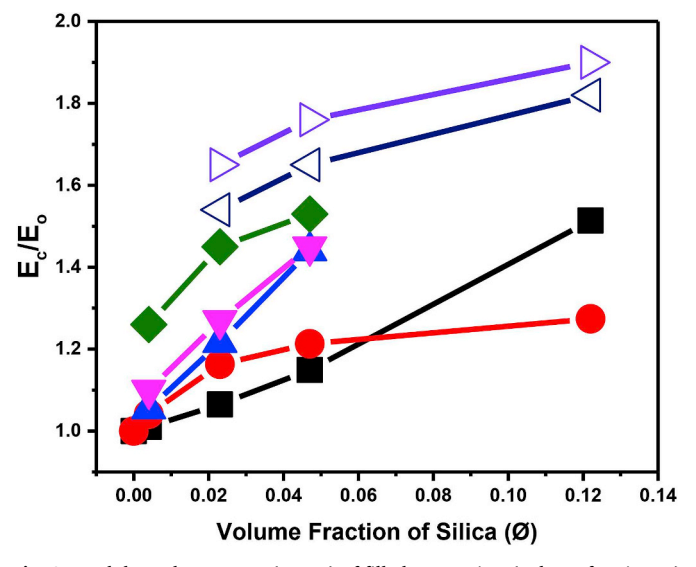


**Fig. 2.** Modulus enhancement (Ec/Eo) of filled composites (volume fraction,  $\varphi$ ) for both predicted (g) and experimental samples  $\bullet$ , C18–SiO<sub>2</sub>;  $\triangle$ ,38k-high density;  $\nabla$ ,73k-high density;  $\Diamond$ ,161k-high density;  $\triangleleft$ ,34.8k-low density;  $\triangleright$ , 134k-low density.

ends was cleaved by refluxing with 20 eq. of AIBN (relative to the moles of RAFT agent) in THF until the yellow color of solution disappeared. The resulting PCP grafted particles without RAFT agent were precipitated into a large amount of methanol and centrifuged at 8,000 rpm for 10 min and redispersed in THF. Differential scanning calorimetry (DSC) analysis of the PCP grafted NPs showed a glass transition temperature of approximately  $-40\,^{\circ}\text{C}$  (Fig. S5).

#### 2.7. Procedure for cleaving grafted polymer from particles

PCP-g-SiO $_2$  particles (20 mg) were dissolved in 2 mL of THF. Aqueous HF (49%, 0.2 mL) was added, and the solution was stirred overnight at r.t. The solution was poured into a PTFE Petri dish and allowed to stand in a fume hood overnight to evaporate the volatiles. The recollected PCP was then subjected to GPC analyses.

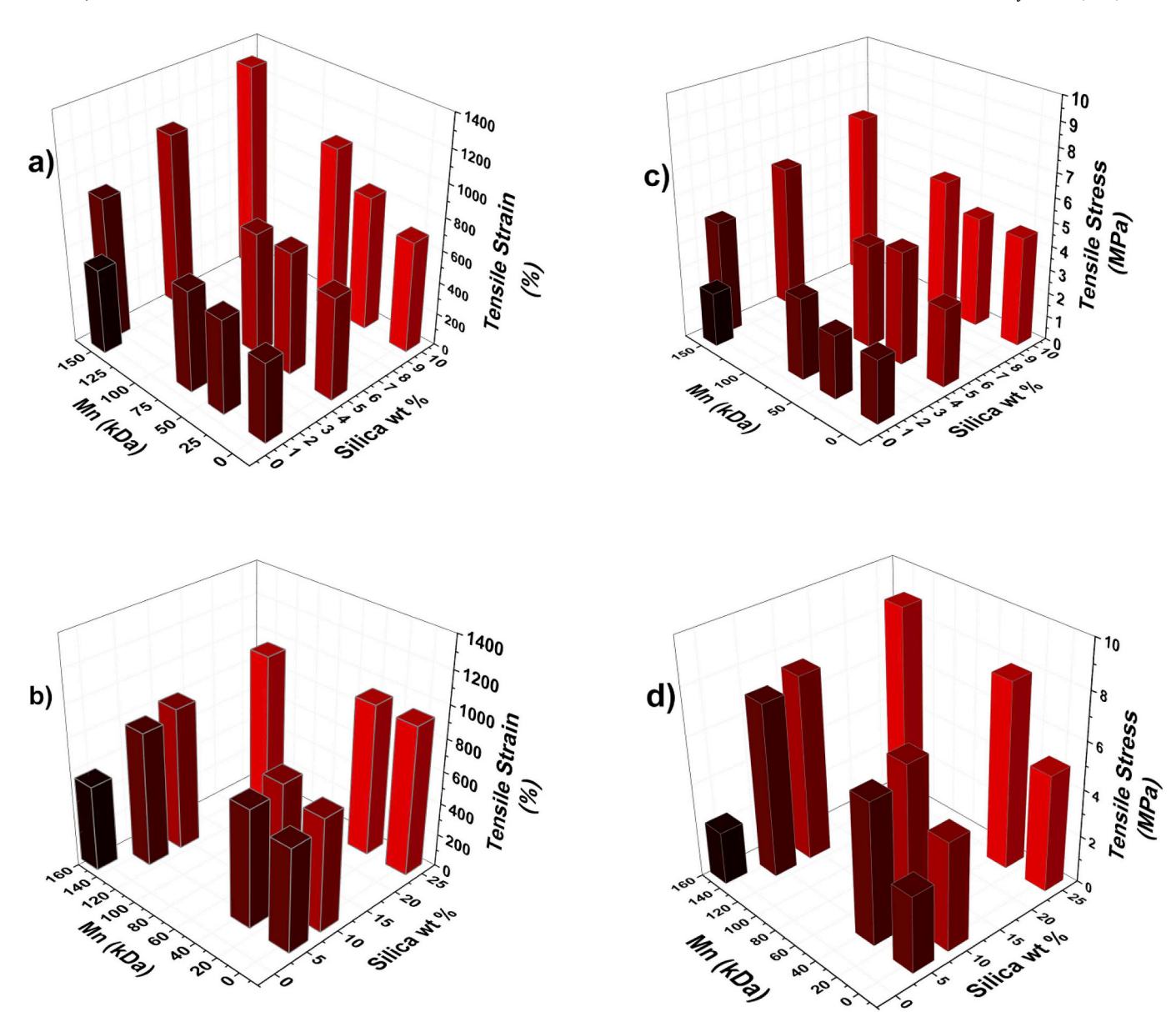


Fig. 3. a) Strain diagram of unfilled polymer and filled composites with different silica loadings and grafted molecular weights of 0.21 ch/nm<sup>2</sup> NPs, b) strain diagram of unfilled polymer and filled composites with different silica loadings and grafted molecular weights of 0.022 ch/nm<sup>2</sup> NPs, c) stress diagram of unfilled polymer and filled composites with different silica loadings and grafted molecular weights of 0.21 ch/nm<sup>2</sup> NPs, d) stress diagram of unfilled polymer and filled composites with different silica loadings and grafted molecular weights of 0.022 ch/nm<sup>2</sup> NPs (see Fig. S7 for individual stress-strain curves).

#### 2.8. Nanocomposite preparation

PCP matrix (1 g) was dissolved in 30 mL of THF and mixed with different loadings of core  $SiO_2$  NP (1, 5, 10, and 25 wt%). Thermogravimetric analysis was used to estimate the neat weight of grafted PCP on  $SiO_2$  NP, then the needed free PCP weight of matrix was added to match projected silica loadings (Table S4). FTIR was also used to confirm the incorporation of the grafted silica NPs into the PCP matrix (Fig. S6, Table S5).

#### 2.9. Curing process of PCP nanocomposites

A solvent mixing technique was used to cure the PCP by adding curing agents. The chloroprene polymer was cured using zinc oxide (5phr), magnesium oxide (2phr), *N*-phenylnaphthalen-2-amine (2phr), stearic acid (0.5phr), and 2-mercaptothiazoline (0.5phr) in THF. After evaporating the solvent samples were hot pressed at 160 °C for 25 min to obtain vulcanized rubber sheet of 0.4 mm thickness [39].

#### 3. Characterization techniques

#### 3.1. Molecular weights

Molecular weights (Mn) and dispersities ( $\mathcal{D}$ ) were determined using a Varian 290 LC gel permeation chromatography (GPC) with a 390 LC multidetector unit, and three Styragel columns. The columns consisted of HR1, HR3, and HR4 in the effective molecular weight ranges of 100–5000, 500–30000, and 5000–500000, respectively. THF was used as eluent at 30 °C and the flow rate was adjusted to 1.0 mL/min. Molecular weights were calibrated with poly(styrene) standards obtained from Polymer Laboratories.

#### 3.2. Transmission electron microscopy

The Transmission Electron Microscopy (TEM) was performed on a Hitachi H8000 TEM at an accelerating voltage of 200 kV. The samples were prepared by cryoultramicrotomy sectioning of crosslinked

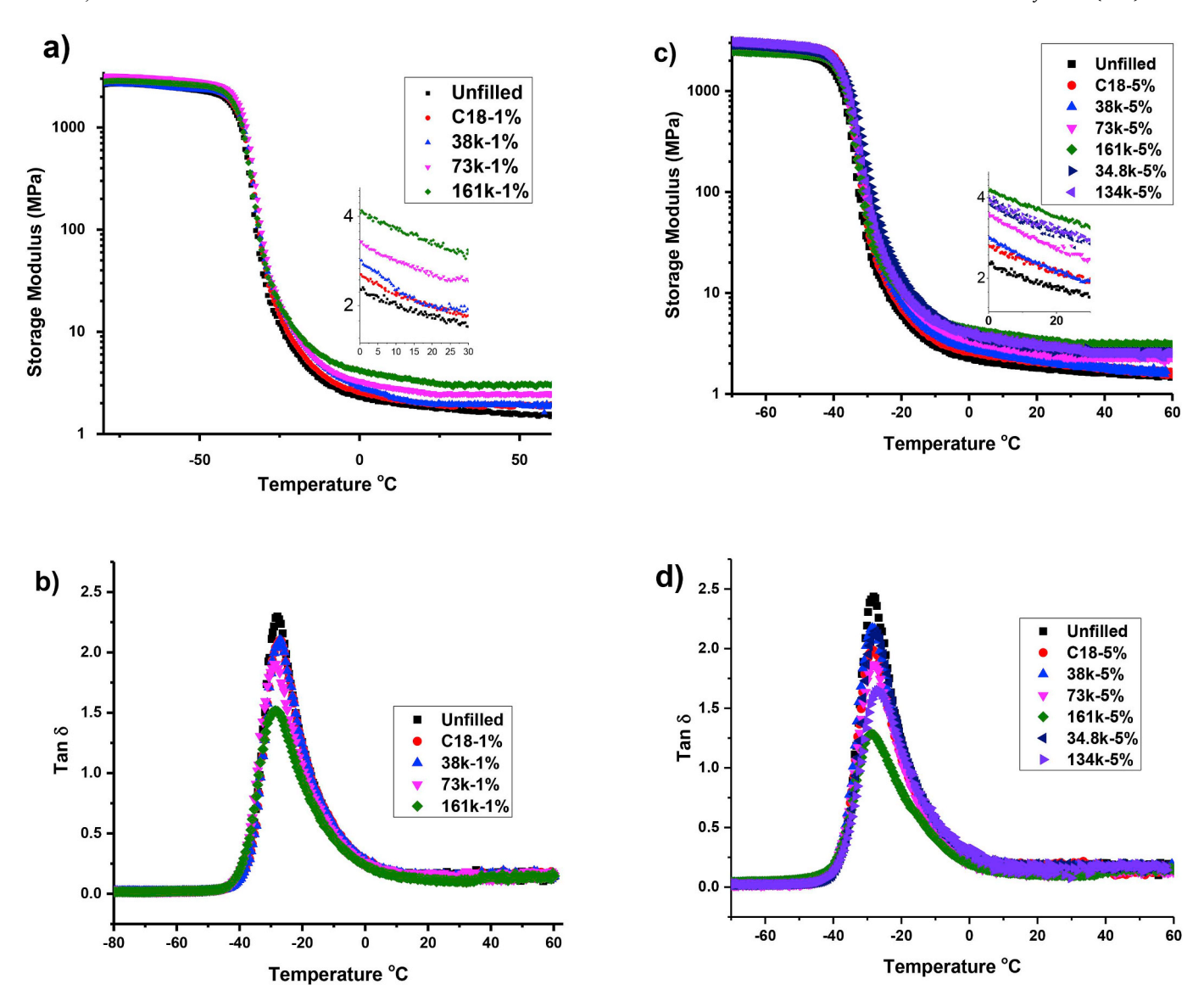


Fig. 4. a, c, e, and g) Storage moduli of unfilled polymer and NP filled composites with different silica loadings and grafted molecular weights at 0.022 and 0.21 ch/nm<sup>2</sup> b, d, f, and h) tan  $\delta$  of unfilled polymer and NP filled composites with different silica loadings and grafted molecular weights at 0.022 and 0.21 ch/nm<sup>2</sup>.

samples in a solution of  $\rm H_2O:DMSO$  30:70, then placed on copper grids. The image was acquired in bright field mode using on objective aperture and a XYZ detector.

#### 3.3. Dynamic mechanical analysis

Dynamic mechanical analysis was performed with an Eplexor 2000 N dynamic measurement system (TA, ARES-RSA3) using a constant frequency of 10 Hz in a temperature range  $-80\,^{\circ}\text{C}$  to  $80\,^{\circ}\text{C}$ . The analysis was done in tension mode. For the measurement of the complex modulus, E\*, a static load of 1% pre-strain was applied and the samples oscillated to a dynamic load of 0.5% strain. Measurements were done with a heating rate of 3  $^{\circ}\text{C/min}$  under nitrogen flow.

#### 3.4. Stress-strain analysis

Tensile tests of samples were carried out using an Instron 5543A material testing machine with crosshead speed 20 mm/min (ASTM D412, ISO 527). Samples were cut into standard dumbbell shapes with neck cross-section dimensions of 5  $\times$  22 mm with 0.4 mm thickness. At least five measurements were recorded, and the average values were reported.

#### 3.5. Swelling measurements

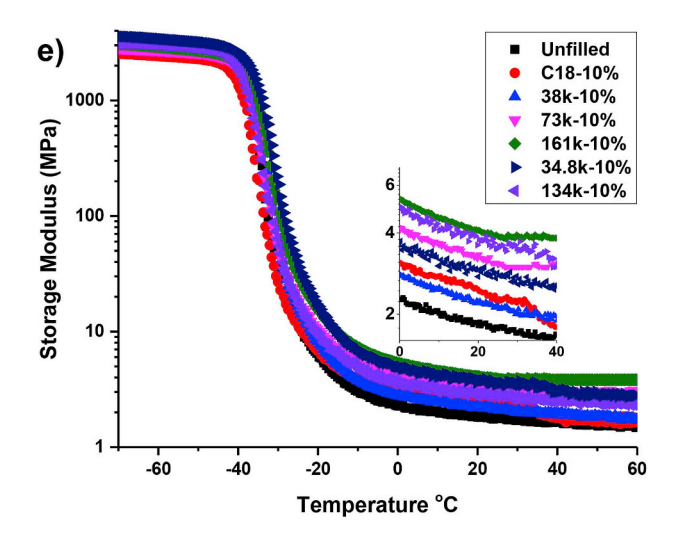
Swelling of the PCP composites was accomplished by soaking the cured sheet of rubber in toluene for seven days at r.t. During the seven days, the toluene was changed daily using fresh toluene. The rubber sheets were removed after seven days and residual solvent on the surface was removed using lab wipes. The weights of the sheets were measured using an analytical balance directly after removal from the residual solvent. The degree of swelling (Q) was determined by the following eq.: [40]:

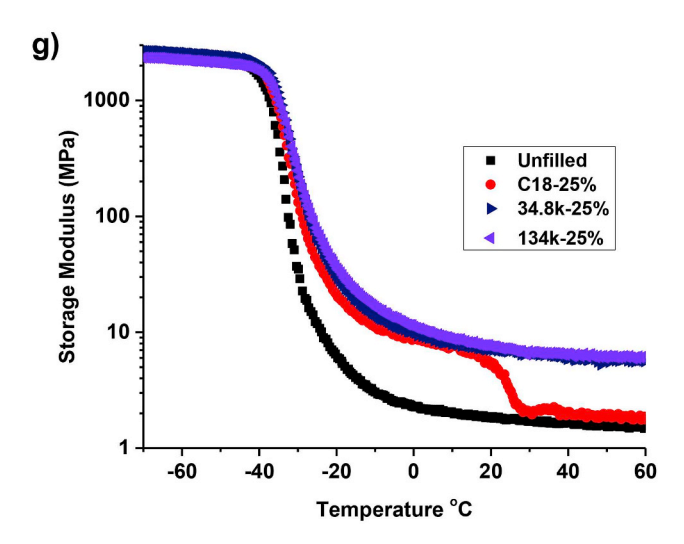
$$Q(\%) = \frac{Ws - Wo}{Wo} * 100 \tag{1}$$

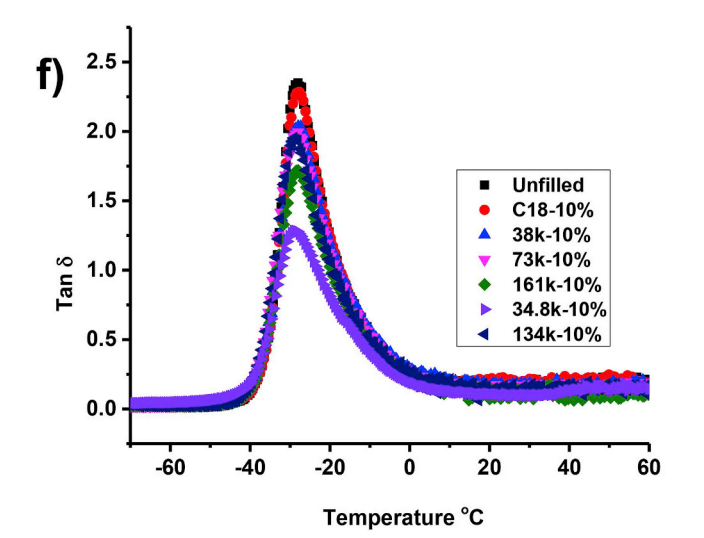
where, Ws is the weight of the sample after swelling and Wo is the weight of sample the before swelling.

#### 3.6. Crosslink density

The crosslink density is the number of effectively elastic chains per unit volume, and can be obtained using the Flory-Rehner eq.: [41,42]:







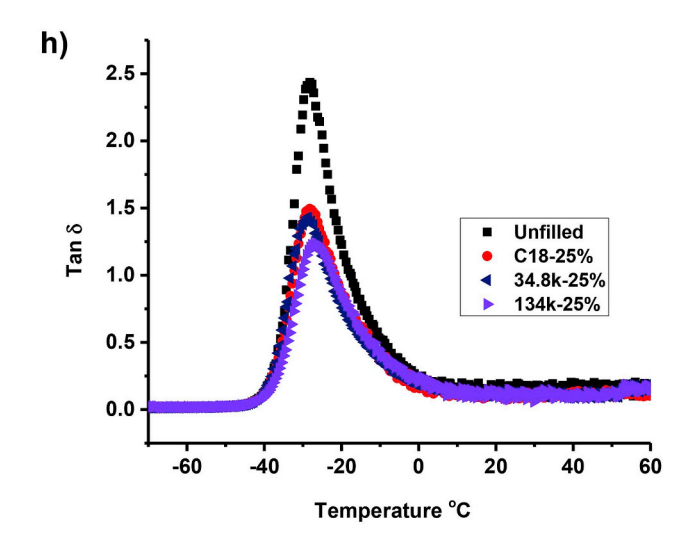


Fig. 4. (continued)

$$v = -[\ln(1 - Vr) + Vr + \chi Vr^2]/Vt \left(Vr^{\frac{1}{3}} - \left(\frac{Vr}{2}\right)\right)$$
 (2)

where Vr is the volume fraction of rubber in the swollen state, Vt is the molar volume of toluene (106.2),  $\chi$  is the effective interaction parameter (CR-toluene), which is (0.342) for the CR-toluene system. All reported values were the average of five test samples after immersion in toluene at 22 °C for one week, and the solvent was replaced daily.

#### 3.7. Small-angle X-ray scattering (SAXS)

X-ray experiments were conducted using a SAXS Lab Ganesha instrument at the South Carolina SAXS Collaborative. A Xenocs GeniX3D microfocus source was used with a Cu target to generate a monochromic beam with a 0.154 nm wavelength. The instrument was calibrated using National Institute of Standards and Technology (NIST) reference material 640c silicon powder with the peak position at  $2\theta=28.44^\circ$  where  $2\theta$  is the total scattering angle. A Pilatus 300 K detector (Dectris) was used to collect the two-dimensional (2D) scattering patterns. All SAXS data were acquired with an X-ray flux of  $\sim 4.1$  M and  $\sim 21.4$  M photons/s incident upon the samples. All data were acquired with 10–15 min measurements. Transmission SAXS was measured with the beam normal to the sample plane. These 2D images

were azimuthally integrated to yield the scattering vector and intensity. The acquired x-ray scattering spectra were well fitted using the Beaucage Unified Fit function [43]:

$$I(q) = G * exp^{\left(-q^2 + \frac{R_g^2}{3}\right)} + B * \left(\frac{q}{erf\left(\frac{q * R_g}{\sqrt{6}}\right)^3}\right)^{-P}$$

where q is the scattering vector, G is the Guinier prefactor,  $R_g$  is the radius of gyration, B is the Porod prefactor, and P is the power law term. Fitting was performed on a Iq vs q coordinate space to evenly weight residual fit error.

#### 3.8. Thermal gravimetric analysis (TGA)

TGA characterization was operated using a TA Instruments Q5000 with a heating rate of 10  $^{\circ}$ C/min form 80  $^{\circ}$ C-800  $^{\circ}$ C under nitrogen flow.

#### 3.9. Differential scanning calorimetry (DSC)

DSC was conducted using a TA Q2000 DSC (TA Instruments) under a nitrogen atmosphere at heating/cooling rates of  $10\,^{\circ}$ C/min.

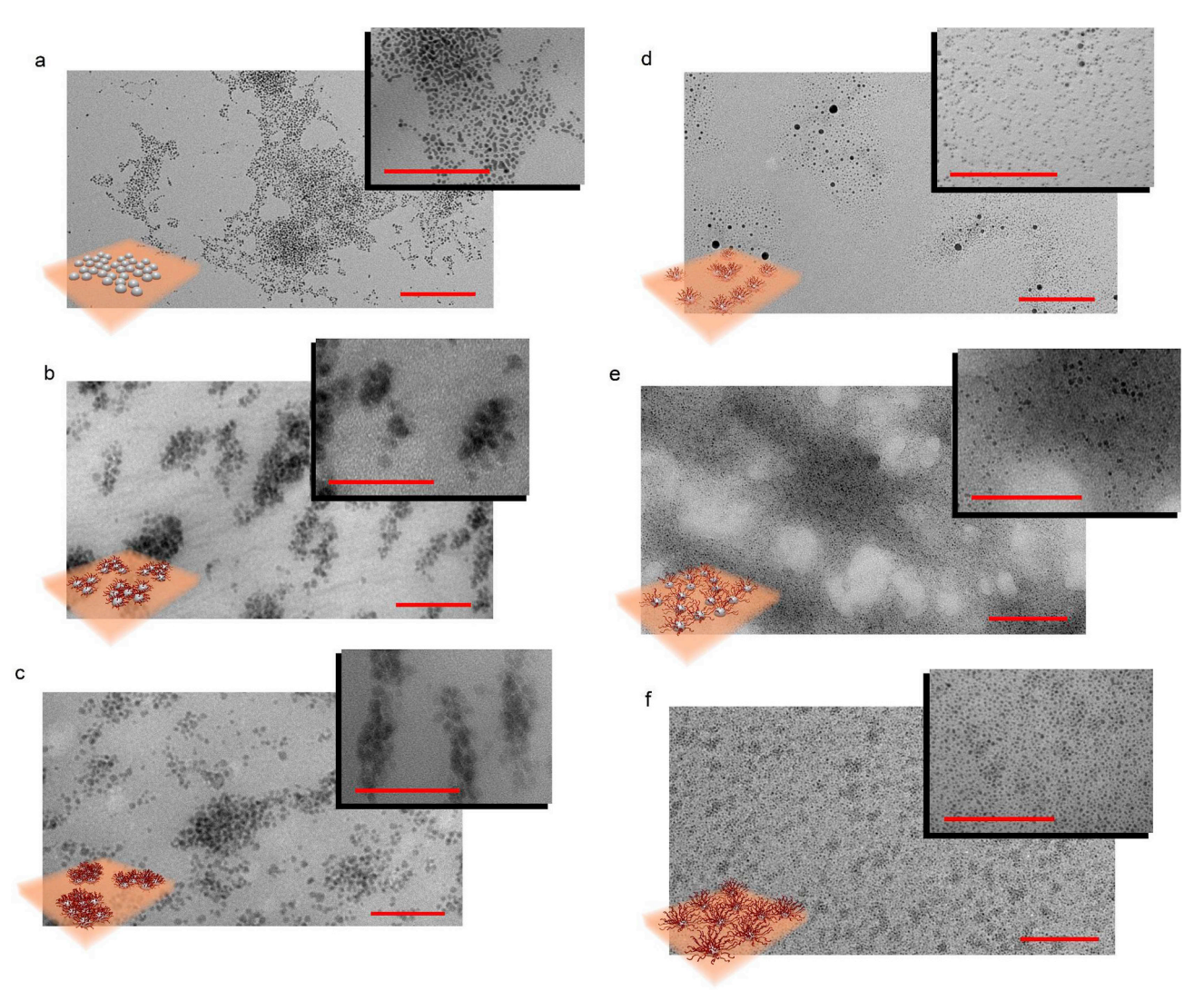


Fig. 5. a) TEM images of PCP nanocomposites with  $10 \text{ wt}\% \text{ SiO}_2 \text{ loading, a}$ ) C18 NPs, b)  $34.8 \text{k-g-SiO}_2 \text{ at } 0.022 \text{ ch/nm}^2$ , c)  $38 \text{k-g-SiO}_2 \text{ at } 0.21 \text{ ch/nm}^2$ , d)  $73 \text{k-g-SiO}_2 \text{ at } 0.22 \text{ ch/nm}^2$ , e)  $134 \text{k-g-SiO}_2 \text{ at } 0.022 \text{ ch/nm}^2$ , f)  $161 \text{k-g-SiO}_2 \text{ at } 0.21 \text{ ch/nm}^2$  (scale bar for all images is 200 nm).

#### 4. Results and discussion

Generally, all fillers that disperse in a rubber interact and play a significant role in the mechanical properties of the elastomeric composites. Our previous work showed that we could controllably polymerize chloroprene from the surface of silica NPs and preliminary mechanical properties were reported on samples made at a single chain density using matrix free composites only [3]. In this work, a more detailed study was conducted using PCP-g-SiO2 NPs (PCP-g-NPs) in an industrial rubber to prepare silica-filled rubber composites to study the effect of SiO<sub>2</sub> NPs on the reinforcement of the rubber composites. This was done at four different loadings and dispersing SiO2 NPs grafted with different PCP molecular weight brushes into a commercial PCP matrix. A series of composites were prepared using SiO2 NPs grafted only with short octadecyl chains (C18), ODDMMS-g-SiO2, to avoid selfagglomeration, and PCP grafted SiO2 NPs using two different graft densities of (0.21 ch/nm<sup>2</sup>) and (0.022 ch/nm<sup>2</sup>) with a broad range of molecular weights (34.8-161 kDa) of grafted PCP. All samples were dispersed in a fixed weight ratio of the industrial matrix with a 150 kDa molecular weight. The details of the samples are listed in Table 1.

The PCP grafted silica NPs were prepared by the surface-initiated RAFT polymerization of chloroprene. After polymerization, the particles were purified using centrifugation to remove small amounts of free PCP chains [3]. NMR analysis showed that the polymer contained 71%

1,4-trans, 23% cis, 1.3% 1,2-additions and 4.7% 3,4-additions, similar to that found in normal free radical polymerization [44,45]. Chloroprene rubbers are often vulcanized using a mixture of metal oxides. In this work, a common recipe was used comprising zinc oxide, magnesium oxide, 2-mercaptothiazoline (accelerator), stearic acid (stabilizer), and *N*-phenylnaphthalen-2-amine. The rubber can be vulcanized in the presence of only zinc oxide, but the use of magnesium oxide is necessary to avoid burning or charring originating from the dehydrochlorination reaction. Under such conditions, the dehydrochlorination reaction of the tertiary allylic positions will occur first, and once the tertiary allylic chlorines (1,2-units) are consumed, the less reactive 3,4-and 1,4-units will undergo dehydrochlorination [41]. Overall, this method has been reported to produce cured rubbers with high flexibility and dimensional stability [23,39,46].

Thermal gravimetric analysis (TGA) was used to confirm the RAFT agent attachment and graft polymerization of chloroprene from the surface of the NPs (Fig. 1). The small weight loss observed for the RAFT agent grafted NPs is representative of the weight loss for the grafted RAFT agent and the nanoparticles surfactant stabilizer. The TGA weight loss result for a 34.8k-25% and 38k-10% samples are also consistent with the calculated value for this chain density. Finally, weight loss for the composite containing dispersed grafted PCP in commercial PCP matrix for the 25 wt % and 10 wt % silica cores is in agreement with the calculations when considering the additional metal oxide curing agents

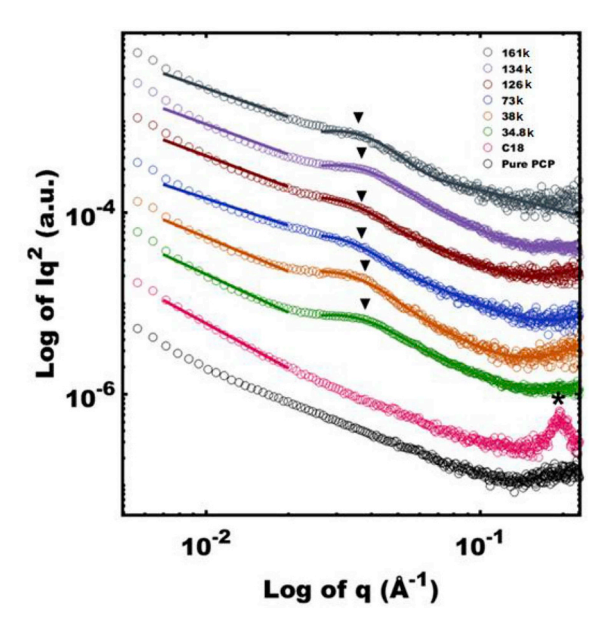


**Fig. 6.** SAXS measurements of grafted nanocomposites with 10 wt% SiO<sub>2</sub> loading. The Bare is C18-g-NPs, and 38, 73, 126, and 161 kDa samples have a chain density of  $0.21 \text{ ch/nm}^2$  while the 34.8 and 134 kDa samples have a chain density of  $0.022 \text{ ch/nm}^2$ . The data were offset vertically for clarity. The Unified fit is shown from  $q = 0.025-0.15 \text{ Å}^{-1}$ .

**Table 2**Unified fit parameters for nanocomposite film SAXS data.

Sample Name	Mn Grafted PCP (kDa)	Graft Density (ch/nm²)	R <sub>g</sub> (nm)	Low-q power law exponent
C18	0	_	_	3.7
34.8k	34.8	0.022	6.3	3.4
38k	38	0.21	6.8	3.3
73k	73	0.21	7.4	3.0
126k <sup>a</sup>	126	0.21	7.3	3.1
134k	134	0.022	6.3	3.1
161k	161	0.21	6.2	3.0

<sup>&</sup>lt;sup>a</sup> Additional sample prepared to expand SAXS data set.

#### (TGA calculations in SI Table S4).

Mechanical properties of the cured composites were evaluated using conventional stress-strain measurements. The increase in modulus for silica reinforced elastomers can be predicted using the Guth-Gold equation [47],

$$\frac{Ec}{Eo} = 1 + 2.5\varphi + 14.1\varphi^2 \tag{3}$$

where Ec and Eo are the tensile moduli of the filled and unfilled composites, respectively. Ec/Eo is termed as the modulus enhancement and  $\varphi$  is the calculated volume fraction of silica in the filled composite.

The experimental data for the modulus enhancement (Ec/Eo) in Fig. 2 were higher than those predicted by the Guth-Gold equation for all of the polymer grafted nanocomposite films. The C18 composite films showed little or minor modulus enhancement, or in the case of the highest loading level tested, a decrease as compared to the theoretical prediction. This suggests that the treatment of silica with grafted chains that can entangle with matrix chains significantly contribute to composite modulus enhancements, beyond the simple creation of a hydrophobic surface layer. Interestingly, samples with lower graft density (unfilled symbols) and high molecular weights of the grafted polymer (e.g., 134k-g-0.022 ch/nm²) showed much greater improvements in the tensile modulus compared to the unfilled composite and the high graft density filled composites (filled symbols) [17,48]. This also supports the chain entanglement hypothesis as a major contributory factor in

improving composite mechanical properties as the long low-density chains will be more efficient in entangling with matrix chains than densely grafted chains. Generally, the strength of the rubber filler interaction appears enhanced by the grafted polymer chains on the silica surface, which results in effectively increasing the filler volume fraction [6,7,22].

Fig. 3 shows the stress-strain data for the unfilled polymer and filled composites with different molecular weights of grafted PCP and loading of silica nanoparticles. For reference, the unfilled, crosslinked PCP properties are plotted as the 0% silica loading using the molecular weight of the resin before crosslinking and the C18–SiO $_2$  grafted particle composites are plotted as the zero value  $M_n$  data. The results show the general expected trend of higher mechanical properties with higher loading levels of silica nanoparticles.

The comparison between the  $C18-SiO_2$  grafted nanocomposite properties and the polymer grafted nanocomposite properties is valuable in pointing to the importance of chain entanglement effects. The C18 grafted chains are effective in creating a hydrophobic layer on the NPs and assisting in dispersing the NPs in the matrix but do not contribute to chain entanglement effects with the matrix polymer. The data for long-chain grafted NPs shows that the mechanical properties were improved across all experimental graft variables and specifically when chain entanglement was most enhanced. These results agree with previous results of NP grafted composites for glassy polymers and general concepts that address the bound layer effect in filled rubbers [23,26–28,31,49].

The importance of graft density and its effects on chain entanglement are also evident from the current study. For example, we can compare the data for 10 wt% silica loaded composites at graft densities of 0.21 ch/nm² and 0.022 ch/nm² with similar molecular weights of grafted chains (161k and 134k, respectively). The stress-at-break for these samples is 6.9 MPa and 7.8 MPa, suggesting that the difference in graft density and its effect on chain entanglement are an important variable of the grafting architecture. For NPs with low graft densities, higher particle loading levels can be attained since the weight percent of grafted chains is smaller than with high graft densities. Thus, further increases in mechanical properties (both tensile strength and modulus, e.g., Fig. 3) were observed at higher silica loading levels for the low graft density NP filled composites.

The effect of PCP-g-NPs on the dynamic mechanical properties of 1, 5, 10, and 25 wt% silica filled nanocomposites is shown in Fig. 4. The storage moduli (E') in the rubbery plateau region showed a continual increase with increasing silica loading. However, the molecular weight of the grafted chains also played an important role in storage modulus. At each of the different chain densities, the storage modulus showed an increase with increasing graft molecular weight. For both chain densities, the highest grafted molecular weights (134k and 161k) yielded the highest values for the storage modulus, as well as the highest values for effective crosslink density. The effects of graft density were also observed at lower molecular weights. Comparison of the samples with 38k grafted chains (high graft density) and 34.8k (low graft density) show that the composites using the 34.8k grafted PCP grafted nanoparticles gave higher room temperature storage moduli at all loading levels. We attribute this to the enhanced chain entanglement of the matrix chains with the low graft density grafted chains that have more space for the matrix chains to penetrate between grafted chains [2]. It should be mentioned that the C18 NP composite samples showed a significant drop in E', particularly noticeable at the higher loading levels. This decrease is likely due to the C18 chains, which have a melting point ~18-20 °C. Thus, the grafted short ligands would not be expected to contribute to a stable entangled state and rubber-silica interaction with the matrix chains at these temperatures [48-50]. A single loss peak was observed for all of the polymer grafted NP composites which were approximately the same as the unfilled crosslinked rubber, also indicating a fairly continuous interface-matrix region [51].

TEM micrographs were acquired to study the dispersion state of the

silica NPs in the PCP nanocomposites. Fig. 5 shows the results for 10% silica loading levels of the grafted NPs for all the molecular weights and graft densities. The short C18 grafted NPs (Fig. 5 a) showed the highest level of agglomeration. At the low polymer molecular weights, small clusters were observed in both the 34.8k (0.022 ch/nm<sup>2</sup>) and 38k (0.21 ch/nm<sup>2</sup>) grafted NP samples (Fig. 5 b and c) due to the incompatibility between the short chains of grafted polymer and longer matrix chains. At the next higher molecular weight, the 73k-g-SiO<sub>2</sub> filled sample (Fig. 5 d) showed improved dispersion with just a moderate distribution of small clusters. At the highest graft molecular weights, the 134k and 161k grafted NPs (Fig. 5 e and f) were dispersed much more effectively due to the improved compatibility and entanglement with matrix chains, consistent with the increase in mechanical properties [16,40]. Energy dispersive X-ray spectroscopy (Fig. S8) further confirmed the highly dispersed state of the high molecular weight grafted nanoparticles in the PCP matrix.

Small-angle X-ray scattering (SAXS) measurements were performed to compare ensemble measurements with localized TEM observations. Kratky plots are presented to highlight subtle changes to the scattering patterns (Fig. 6 and Fig. S9). The data were well fitted using the Beaucage unified model [43]. The fit parameters are presented in Table 2. SAXS data from the polymer grafted nanoparticles were largely similar, inflection points for each sample are marked. Considering the sample with 34.8 kDa PCP and a graft density of 0.21 chains/nm<sup>2</sup> as a representative sample, the 6.3 nm radius of gyration corresponded to a sphere diameter of 16.3 nm (2\*R<sub>g</sub>\*(5/3)<sup>0.5</sup>), consistent with nominal 15 nm SiO<sub>2</sub> nanoparticle diameter. This sample did not exhibit an apparent structure factor peak that was indicative of extensive aggregation in prior studies [52]. Well-dispersed nanoparticle composites were previously shown to yield a low-q scattering power law exponent of 2.0. However, this sample exhibited a higher exponent of 3.4, suggestive of some aggregation. The TEM observations were consistent with this interpretation where both dispersed and somewhat aggregated nanoparticles were observed. Similar fit results were obtained for samples with lower molecular weight grafted chains. However, for those composites using nanoparticles with grafted chain molecular weights ≥73 kDa the power law exponent decreased to ~3.0, suggestive of improved dispersion (Table 2). The SAXS profile for PCP with 10 wt% of C18 SiO2-NP loaded films did not exhibit an inflection point and the fit function did not converge to a unique solution. This sample exhibited a peak near  $q = 1.96 \,\text{nm}^{-1}$  (indicated with asterisk), suggestive of surfactant aggregation and consistent with scattering from e.g. stearic acid [53].

#### 5. Conclusions

A study on the reinforcement of polychloroprene (PCP) was performed using PCP grafted silica nanoparticles, prepared by the polymerization of chloroprene from the surface of silica via surface-initiated RAFT polymerization. The results were compared to short C18 grafted NPs, which was used to create a hydrophobic layer on the silica. Comparatively, the cured composites with the C18 grafted NPs showed lower mechanical properties and poor dispersion in the PCP matrix. Samples with grafted PCP showed higher mechanical properties and better dispersion due to the improved interactions and chain entanglement of the matrix with the grafted polymer chains. Two different graft densities were studied representing the low and high graft density regimes. The cured composites with low graft density NPs exhibited greater enhancement and at lower grafted molecular weights due to the penetration of matrix chains into the polymer brushes. The mechanical properties generally improved by increasing the silica loading from 1 to 25 wt%. The modified rubber produces a strong nanocomposite which will be useful in many applications. The control and variation of grafted molecular weight and chain density of grafted polymer could be a very effective technique to convey improved nanocomposite properties for practical applications.

#### Acknowledgements

We acknowledge the support from the SC SmartState program. Also, ZMA acknowledges the funding and support from the Wasit University-Iraqi ministry of higher education and scientific research. ZM acknowledges support by the National Science Foundation EPSCoR Program under NSF Award #OIA-1655740. MS acknowledges support by the National Science Foundation (DMR-1752615). This work made use of the South Carolina SAXS Collaborative, supported by the NSF Major Research Instrumentation program (DMR-1428620). We would like to thank Columbia University Electron Microscopy Lab and Dr. Amirali Zangiabadi for help with the EDS measurements.

#### Appendix A. Supplementary data

Supplementary data to this article can be found online at https://doi.org/10.1016/j.polymer.2019.03.031.

#### References

- S. Faraji, M.F. Yardim, D.S. Can, A.S. Sarac, Characterization of polyacrylonitrile, poly(acrylonitrile-co-vinyl acetate), and poly(acrylonitrile-co-itaconic acid) based activated carbon nanofibers, J. Appl. Polym. Sci. 134 (2017) 1–10, https://doi.org/ 10.1002/app.44381.
- [2] Y. Huang, Y. Zheng, A. Sarkar, Y. Xu, M. Stefik, B.C. Benicewicz, Matrix-free polymer nanocomposite thermoplastic elastomers, Macromolecules 50 (2017) 4742–4753, https://doi.org/10.1021/acs.macromol.7b00873.
- [3] Y. Zheng, Z.M. Abbas, A. Sarkar, Z. Marsh, M. Stefik, B.C. Benicewicz, Surface-initiated reversible addition-fragmentation chain transfer polymerization of chlor-oprene and mechanical properties of matrix-free polychloroprene nanocomposites, Polymer (Guildf) 135 (2018) 193–199, https://doi.org/10.1016/j.polymer.2017.
- [4] D. Zhao, M. Di Nicola, M.M. Khani, J. Jestin, B.C. Benicewicz, S.K. Kumar, Self-Assembly of monodisperse versus bidisperse polymer-grafted nanoparticles, ACS Macro Lett. 5 (2016) 790–795, https://doi.org/10.1021/acsmacrolett.6b00349.
- [5] D. Hosler, S.L. Burkett, M.J. Tarkanian, Prehistoric polymers: rubber processing in ancient mesoamerica, Science 284 (1999) 1988–1991, https://doi.org/10.1126/ science.284.5422.1988.
- [6] A. bin Othman, M.J. Gregory, Stiffening effect of carbon black: its interpretation by a modified Guth-Gold equation, J. Nat. Rubber Res. 3 (1988) 7–20.
- [7] M. Qu, F. Deng, S.M. Kalkhoran, A. Gouldstone, A. Robisson, K.J. Van Vliet, Nanoscale visualization and multiscale mechanical implications of bound rubber interphases in rubber–carbon black nanocomposites, Soft Matter 7 (2011) 1066, https://doi.org/10.1039/c0sm00645a.
- [8] M.A. Mutar, Q.K. Mugar, The study of the development of natural rubber blends using different types of polymers and fillers on the mechanical and chemical properties of the vulcanizates, J. Nat. Sci. Res. 4 (2014) 60–73 http://www.iiste. org/Journals/index.php/JNSR/article/view/18545.
- [9] K.S. Merza, H.D. Al-Attabi, Z.M. Abbas, H.A. Yusr, Comparative study on methods for preparation of gold nanoparticles, Green Sustain. Chem. 2 (2012) 26–28, https://doi.org/10.4236/gsc.2012.21005.
- [10] Y. Mao, S. Li, H.J. Ploehn, The role of interlayer grafting on the mechanical properties of magadiite/styrene-butadiene rubber composites, J. Appl. Polym. Sci. 134 (2017) 1–11, https://doi.org/10.1002/app.45025.
- [11] S.N. Bhattacharya, M.R. Kamal, R.K. Gupta, Polymeric Nanocomposites Theory and Practice, Carl Hanser Publishers, Munich, 2007, https://doi.org/10.3139/ 078044641878
- [12] M. Giovino, J. Pribyl, B. Benicewicz, R. Bucinell, L. Schadler, Mechanical properties of polymer grafted nanoparticle composites, Nanocomposites 0 (2019) 1–9, https://doi.org/10.1080/20550324.2018.1560988.
- [13] H. Skaff, T. Emrick, Reversible addition fragmentation chain transfer (RAFT) polymerization from unprotected cadmium selenide nanoparticles, Angew. Chem. Int. Ed. 43 (2004) 5383–5386, https://doi.org/10.1002/anie.200453822.
- [14] E.H. Discekici, C.W. Pester, N.J. Treat, J. Lawrence, K.M. Mattson, B. Narupai, E.P. Toumayan, Y. Luo, A.J. McGrath, P.G. Clark, J. Read De Alaniz, C.J. Hawker, Simple benchtop approach to polymer brush nanostructures using visible-lightmediated metal-free atom transfer radical polymerization, ACS Macro Lett. 5 (2016) 258–262, https://doi.org/10.1021/acsmacrolett.6b00004.
- [15] Pedro Henrique Cury Camargo, Kestur Gundappa Satyanarayana, Fernando Wypych, Nanocomposites: synthesis, structure, properties and new application opportunities, Mater. Res. 12 (2009) 1–39, https://doi.org/10.1590/ S1516-14392009000100002.
- [16] J.B. Hooper, K.S. Schweizer, Theory of phase separation in polymer nanocomposites, Macromolecules 39 (2006) 5133–5142, https://doi.org/10.1021/ma060577m.
- [17] J.F. Moll, P. Akcora, A. Rungta, S. Gong, R.H. Colby, B.C. Benicewicz, S.K. Kumar, Mechanical reinforcement in polymer melts filled with polymer grafted nanoparticles, Macromolecules 44 (2011) 7473–7477, https://doi.org/10.1021/ ma201200m.
- [18] C. Li, B.C. Benicewicz, Synthesis of well-defined polymer brushes grafted onto silica

nanoparticles via surface reversible addition - fragmentation chain transfer polymerization, Macromolecules 38 (2005) 5929–5936, https://doi.org/10.1021/

- [19] C. Li, J. Han, C.Y. Ryu, B.C. Benicewicz, A versatile method to prepare RAFT agent anchored substrates and the preparation of PMMA grafted nanoparticles a versatile method to prepare RAFT agent anchored substrates and the preparation of PMMA grafted nanoparticles, Macromolecules 39 (2006) 3175–3183, https://doi.org/10. 1021/ma051983t.
- [20] K.E. Polmanteer, Reinforcement studies effects of silica structure on properties and crosslink density, Rubber Chem. Technol. 48 (1975) 795–809.
- [21] G. Heinrich, M. Kluppel, T.A. Vilgis, Reinforcement of elastomers, Curr. Opin. Solid State Mater. Sci. 6 (2002) 195–203.
- [22] D. Maillard, S.K. Kumar, B. Fragneaud, J.W. Kysar, A. Rungta, B.C. Benicewicz, H. Deng, L.C. Brinson, J.F. Douglas, Mechanical properties of thin glassy polymer films filled with spherical polymer-grafted nanoparticles, Nano Lett. 12 (2012) 3909–3914, https://doi.org/10.1021/nl301792g.
- [23] B.P. Kapgate, C. Das, A. Das, D. Basu, S. Wiessner, U. Reuter, G. Heinrich, Reinforced chloroprene rubber by in situ generated silica particles: evidence of bound rubber on the silica surface, J. Appl. Polym. Sci. 133 (2016) 1–10, https://doi.org/10.1002/app.43717.
- [24] L.B. Tunnicliffe, J.J.C. Busfiel, Reinforcement of rubber and filler network dynamics at small strains, Adv. Polym. Sci. 275 (2016) 71–102, https://doi.org/10.1007/12.
- [25] W.H. Carothers, I. Williams, A.M. Collins, J.E. Kirby, Acetylene polymers and their derivatives. II. A new synthetic rubber: chloroprene and its polymers, J. Am. Chem. Soc. 53 (1931) 4203–4225, https://doi.org/10.1021/ja01362a042.
- [26] S.R. Scagliusi, S.G. Araújo, L. Landini, A.B. Lugão, Study of properties of chloroprene rubber devulcanizate by radiation in microwave, Int. Nucl. Atl. Conf. Rio Janeiro, RJ, Brazil, vol 41, 2009.
- [27] E.M. Dannenberg, Bound rubber and carbon black reinforcement, Rubber Chem. Technol. 59 (1986) 512–524, https://doi.org/10.5254/1.3538213.
- [28] H. Xu, Y. Song, E. Jia, Q. Zheng, Dynamics heterogeneity in silica-filled nitrile butadiene rubber, J. Appl. Polym. Sci. 135 (2018) 63–67, https://doi.org/10.1002/ app.46223.
- [29] J. Lawrence, J.T. Pham, D.Y. Lee, Y. Liu, A.J. Crosby, T. Emrick, Highly conductive ribbons prepared by stick-slip assembly of organosoluble gold nanoparticles, ACS Nano 8 (2014) 1173–1179.
- [30] A.M. Smith, K.A. Johnston, S.E. Crawford, L.E. Marbella, J.E. Millstone, Ligand density quantification on colloidal inorganic nanoparticles, Analyst 142 (2017) 11–29, https://doi.org/10.1039/c6an02206e.
- [31] S.K. Kumar, N. Jouault, B. Benicewicz, T. Neely, Nanocomposites with polymer grafted nanoparticles, Macromolecules 46 (2013) 3199–3214, https://doi.org/10. 1021/ma4001385.
- [32] B. Natarajan, T. Neely, A. Rungta, B.C. Benicewicz, L.S. Schadler, Thermomechanical properties of bimodal brush modified nanoparticle composites, Macromolecules 46 (2013) 4909–4918. https://doi.org/10.1021/ma400553c.
- [33] P. Akcora, H. Liu, S.K. Kumar, J. Moll, Y. Li, B.C. Benicewicz, L.S. Schadler, D. Acehan, A.Z. Panagiotopoulos, V. Pryamitsyn, V. Ganesan, J. Ilavsky, P. Thiyagarajan, R.H. Colby, J.F. Douglas, Anisotropic self-assembly of spherical polymer-grafted nanoparticles, Nat. Mater. 8 (2009) 354–359, https://doi.org/10. 1038/mmat2404.
- [34] N. Pullan, M. Liub, P.D. Topham, Reversible addition–fragmentation chain transfer polymerization of 2-chloro-1,3-butadiene, Polym. Chem. 4 (2013) 2272–2277, https://doi.org/10.1039/c3pv21151g.
- [35] M.M. Khani, Z.M. Abbas, B.C. Benicewicz, Well-defined polyisoprene-grafted silica

- nanoparticles via the RAFT process, J. Polym. Sci. Part A Polym. Chem. (2017) 1–9, https://doi.org/10.1002/pola.28514.
- [36] S.K. Kumar, B.C. Benicewicz, R.A. Vaia, K.I. Winey, 50th anniversary perspective: are polymer nanocomposites practical for applications? Macromolecules 50 (2017) 714–731, https://doi.org/10.1021/acs.macromol.6b02330.
- [37] C. Li, J. Han, C.Y. Ryu, B.C. Benicewicz, A versatile method to prepare RAFT agent anchored substrates and the preparation of PMMA grafted-nanoparticles, Macromolecules 39 (2006) 3175–3183, https://doi.org/10.1021/ma051983t.
- [38] B. Benicewicz, L. Wang, M. Mohammadkhani, Butadiene-Derived Polymers Grafted Nanoparticles and Their Methods of Manufacture and Use vol 9249025, U.S.P., 2016
- [39] R.N. Datta, Rubber Curing Systems, Rapra Technology Limited, Shropshire, 2002, https://doi.org/10.1201/9781420007183.
- [40] L.H. Sperling, L.H. Sperling, Introduction to Physical Polymer Science, fourth ed., John Wiley & Sons, Inc., New Jersey, 2015.
- [41] J.L. Valentín, J. Carretero-González, I. Mora-Barrantes, W. Chassé, K. Saalwächter, Uncertainties in the determination of cross-link density by equilibrium swelling experiments in natural rubber, Macromolecules 41 (2008) 4717–4729, https://doi. org/10.1021/ma8005087
- [42] L. Ibarra, C. Chamorro, Short fiber-elastomer composites. Effects of matrix and fiber level on swelling and mechanical and dynamic properties, J. Appl. Polym. Sci. 43 (1991) 1805–1819, https://doi.org/10.1002/app.1991.070431004.
- [43] T. Hashimoto, S. Koizumi, Combined Small-Angle Scattering for Characterization of Hierarchically Structured Polymer Systems over Nano-To-Micron Meter: Part I Experiments, Elsevier B.V., 2012, https://doi.org/10.1016/B978-0-444-53349-4. 00297-1.
- [44] V. Arjunan, S. Subramanian, S. Mohan, Vibrational spectroscopic studies on trans-1,4-polychloroprene, Turk. J. Chem. 27 (2003) 423–431.
- [45] G. Moad, Reversible addition-fragmentation chain transfer (co)polymerization of conjugated diene monomers: butadiene, isoprene and chloroprene, Polym. Int. 66 (2017) 26-41, https://doi.org/10.1002/pi.5173.
- [46] Y. Chokanandsombat, C. Sirisinha, MgO and ZnO as reinforcing fillers in cured polychloroprene rubber, J. Appl. Polym. Sci. 128 (2013) 2533–2540, https://doi. org/10.1002/app.38579.
- [47] E. Guth, Theory of filler reinforcement, J. Appl. Phys. 16 (1945) 20–25, https://doi. org/10.1063/1.1707495.
- [48] P. Tao, Y. Li, A. Rungta, A. Viswanath, J. Gao, B.C. Benicewicz, R.W. Siegel, L.S. Schadler, TiO2 nanocomposites with high refractive index and transparency, J. Mater. Chem. 21 (2011) 18623, https://doi.org/10.1039/c1jm13093e.
- [49] C.M. Roland, Reinforcement of elastomers, Ref. Modul. Mater. Sci. Mater. Eng. (2016) 2475–2480. https://doi.org/10.1016/8978-0-12-803581-8.02163-9 1.
- [50] J.M. Torres, C.M. Stafford, B.D. Vogt, Impact of molecular mass on the elastic modulus of thin polystyrene films, Polymer (Guildf). 51 (2010) 4211–4217, https://doi.org/10.1016/j.polymer.2010.07.003.
- [51] C.G. Robertson, C.J. Lin, R.B. Bogoslovov, M. Rackaitis, P. Sadhukhan, J.D. Quinn, C.M. Roland, Flocculation, reinforcement, and glass transition effects in silica-filled styrene-butadiene rubber, Rubber Chem. Technol. 84 (2011) 507–519, https://doi. org/10.5254/1.3601885
- [52] P. Akcora, S.K. Kumar, V. García Sakai, Y. Li, B.C. Benicewicz, L.S. Schadler, Segmental dynamics in PMMA-grafted nanoparticle composites, Macromolecules 43 (2010) 8275–8281, https://doi.org/10.1021/ma101240j.
- [53] R.V. Haware, B.P. Vinjamuri, A. Sarkar, M. Stefik, W.C. Stagner, Deciphering magnesium stearate thermotropic behavior, Int. J. Pharm. 548 (2018) 314–324, https://doi.org/10.1016/j.ijpharm.2018.07.001.